Impact Factor (SJIF): 3.632

International Journal of Advance Research in Engineering, Science & Technology

e-ISSN: 2393-9877, p-ISSN: 2394-2444

Volume 3, Issue 7, July-2016

Effects of magnesium substitution in hydroxyapatite and its coating on stainless steel 316L

Vivek Rajput, Dr. Uma Batra

([1,2]Materials and Metallurgical Engineering Department, PEC University of Technology)

Abstract- *In this work, hydroxyapatite (HA) and magnesium doped hydroxyapatite nanopowder (Mg2HA and Mg4HA) were synthesized by the sol-gel method using precursor calcium nitrate tetra-hydrate (CNT) for calcium, tri-ethyl phosphate (TEP) for phosphorous and magnesium nitrate hexa-hydrate for magnesium and their coatings were deposited on stainless steel 316L using dip coating technique. The powders were calcined at 400ºC and coated samples were sintered at 400ºC. The Ca/P ratio of the synthesized HA and (Ca+Mg)/P ratio of Mg2HA and Mg4HA nanoparticles were maintained in the range of 1.58–1.67. Various characterization techniques were used to study the compositional structure, functionality and phase changes of powders and microstructure of coatings by using XRF, FTIR, XRD and FE-SEM respectively. The mechanical properties of coatings like surface roughness, micro hardness and adhesion strength were also characterized. Potentiodynamic linear polarization was also done to study the corrosion behavior of coated samples. XRF confirms that magnesium has been doped successfully and HA, Mg2HA and Mg4HA coatings were successfully and uniformly deposited on 316L SS. Mg4HA showed the good mechanical behavior like its micro hardness and adhesion strength was high and low surface roughness. Corrosion study reveals that Mg4HA has good corrosion resistance.*

Keywords: *Hydroxyapatite, Magnesium, Sintering, Mechanical Properties*

1. Introduction

Among the various implant materials, 316L SS is widely used as a biomedical implant material, particularly for orthopedic and dental implants due to its mechanical properties (strength, ductility) and low cost [1]. However 316L SS is not bioactive and therefore is not osteointegrative. In order to ensure the corrosion resistance, osteo-integration, and biocompatibility of 316L SS its surface is usually treated with osteo-conductive or osteo-integrating biomaterials such as calcium phosphate ceramics [2]. HA has a composition which is similar to the mineral composition of the bone. Bioactive HA coating on 316L SS implants is able to stimulate the bone growth and affixation to the implant surface during the early stage of implantation. HA is widely used in orthopedic and reconstructive surgery thanks to its excellent bioactivity and biocompatibility with the human body [3]. However, the biological apatites contain several species as traces such as F^{-}, Cl^{-}, Na^{+}, $Sr^{2+,}$ Mg^{2+} etc. Therefore the incorporation of one or several of these ions into HA structure should improve its biocompatibility and bioactivity [4,5] and affects its physical and chemical properties such as crystallinity, thermal stability, solubility and osteo conductivity [6]. It has been suggested that magnesium directly stimulates osteoblast proliferation. Incorporation of Mg^{2+} into hydroxyapatite decreases its crystallinity and improves the biological performances, i.e. good bioactivity and better cell behavior. The biodegradable nature of magnesium makes it a most highlighted and interesting addition to HAP [6]. Mg-HA coating favors the adhesion and proliferation of the cells. Hence, it is thought worthwhile to synthesize and characterize Mg^{2+} substituted hydroxyapatite and it is to be coated on stainless steel using dip coating technique.

In this study, magnesium doped hydroxyapatite coatings were developed on 316L SS using dip coating technique. The Powders and coatings were characterized in terms of phase and elemental composition, functionality, microstructure study and mechanical stability.

2. Materials and methods

2.1 Preparation of 316L SS specimens

Composition of 316L SS is shown in Table 2.1. Samples were cut into 20mm × 20mm size from 316L SS sheet. The burr was removed by grinding the surface. The samples were polished by emery papers which are in sequence 120, 220, 320, 400, 600,800 and 1000 grit to get flat and scratch free surface and then the samples were polished with Aluminum oxide 500µm mesh size. After polishing 316L SS were degreased, washed with distilled water and were placed in ultrasonic bath and then rinsed in acetone before coating.

Table 1: Chemical composition (Wt.%) of AISI 316 L stainless steel.

Element	C	Mn	P	Si	Cr	Ni	Mo	N	Cu	Fe
Composition	0.3	2	0.025	0.75	16.9	11.2	2.1	0.06	0.03	Balance

2.2 Synthesis using sol-gel process

The synthesis process of HA, Mg2HA and Mg4HA samples has been done using sol–gel route and all the chemicals used in the synthesis has been purchased from Sigma-Aldrich. Calcium nitrate tetra-hydrate ($Ca(NO_3)^2.4H_2O$, CNT), tri-ethyl phosphite ($C_6H_{15}O_3P$, TEP), magnesium nitrate hexa-hydrate ($Mg(NO_3)^2.6H_2O$) were used as starting reagents. For HA Ca/P molar ratio was maintained at 1.67 and for Mg2HA and Mg4HA (Ca+Mg)/P molar ratio was maintained at 1.67. To prepare HA nanopowder, 1M solution of CNT was prepared by dissolving CNT in ethanol and 0.6M solution of TEP was prepared by dissolving TEP in ethanol separately. Then, the precursors were hydrolyzed by stirring at 800 rpm for 20 min at 37ºC. Then 1M CNT solution was added drop wise (3 ml/min) to the 0.6M TEP solution and during addition solution was stirred vigorously at 800 rpm. After the addition, the stirring was done for 30 minutes at 800 rpm.

To synthesize the Mg2HA and Mg4HA nanopowders, 0.02M MgNT was dissolved in 0.98M CNT for Mg2HA and 0.04M MgNT was dissolved in 0.96M CNT for Mg4HA. The rest procedure was followed as for synthesis of HA. The sols were aged for 24 hrs followed by their drying at 80ºC followed by calcination at 400ºC.

2.3 Preparing coating on substrate

The coatings were deposited by dip coating technique by using parameters: (dipping speed=100 mm/min, withdrawal speed=30 mm/min, dipping time= 4 min. The coatings were dried at 95ºC for 15 minutes and then sintered at 400ºC for 2 hrs.

Fig 1 gives the consolidated protocol used in this work to synthesize HA, Mg2HA and Mg4HA powders and their coatings on 316L SS.

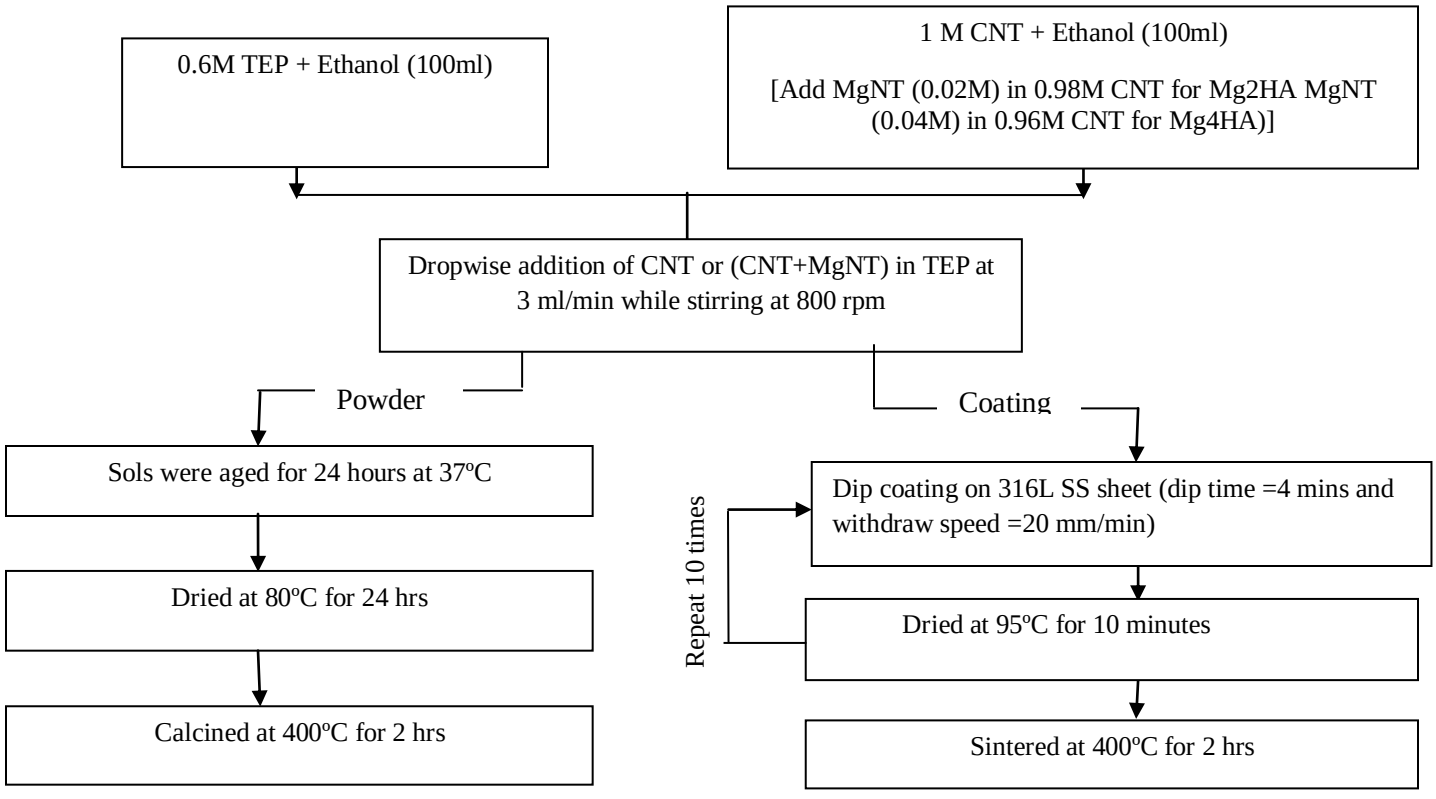

Fig 1: Protocol for Synthesis and coatings of HA and Mg substituted HA

2.4 Characterization

The effect of magnesium substitution on the different functional groups was identified with Fourier Transform Infrared Spectroscopy (FTIR, Perkin Elmer, RZX, USA) in the region of 400-4000 cm^{-1}. The crystal structure and phase composition of samples was determined using an X-ray diffraction (XRD, Rigaku, Ultima IV) with Cu-K_α radiation, operating at 40kV and 40 mA. A detailed scan was done over the 2θ range of 10^o to 80^o with a step size of 0.01^o. The elemental composition was determined with X-Ray Fluorescence (XRF, Bruker, S8 Tiger, Germany). The Microstructural features and uniformity of coating was determined using Field Emission Scanning Electron Microscope (FE-SEM, Hitachi, SU8010).

The electrochemical corrosion behavior testing of HA, Mg2HA and Mg4HA was performed in simulated body fluid (SBF) at the electrochemical workstation (Metrohm Autolab, PGSTAT 302N). Corrosion rate of all the samples was analysed with the help of Tafel extrapolation methods. The surface roughness was determined with a using surface testing machine (Surftest, Mitutoyo, SJ-400) for a cut-off of 0.8 mm. An average five measurements carried out at different locations was taken. The micro hardness test on coated samples was conducted using a Vicker's micro hardness tester (Huayin, HV-1000 V,) with a load of 10 gm and a dwelling time of 10 sec. The adhesion strength of the coating layer was calculated from the Vickers hardness by using the following equation:

$$Adhesion\ Strength = \left(\frac{VHN}{3}\right) 0.1^n \qquad (1)$$

3. Results and Discussions

3.1 Structural Characterization by FTIR, XRD and XRF

The FT-IR spectra of HA, Mg2HA and Mg4HA are shown in Fig. 2. The spectrum of FTIR of HA prepared by sol-gel method sintered at 400ºC for 2 hours is showing the vibration of PO_4 at 1094 cm^{-1}, 1027-1073 cm^{-1}, 963 cm^{-1}, 603 cm^{-1}, 570 cm^{-1}, 470 cm^{-1} frequency shows the stability of phosphor in tetrahedral bonded with oxygen. The presence of HPO_4^{2-} peak in the spectrum is the conformation of calcium deficient hydroxyapatite in structure. CO_3^{2-} in the spectrum shows that C is absorbed form the environment during synthesis of HA. The spectrum of Mg-HA in comparison to the HA shows the shift of the OH peak from 3540, 633 cm^{-1} to 3572, 670 cm^{-1}. The FTIR spectra of the different concentration of Mg2HA and Mg4HA are similar to those reported for HA. The vibrations at 1095 cm^{-1}, 1027-1073 cm^{-1}, 964 cm^{-1}, 603 cm^{-1}, 574 cm^{-1}, 471 cm^{-1} of PO_4^{2-} show the stability of the apatite. Not much significant changes in the shapes and intensities of the peaks were observed for all the samples which indicate that no structural modification of HA due to the substitution of Mg was observed [9]. FTIR results confirmed the formation of hydroxyapatite.

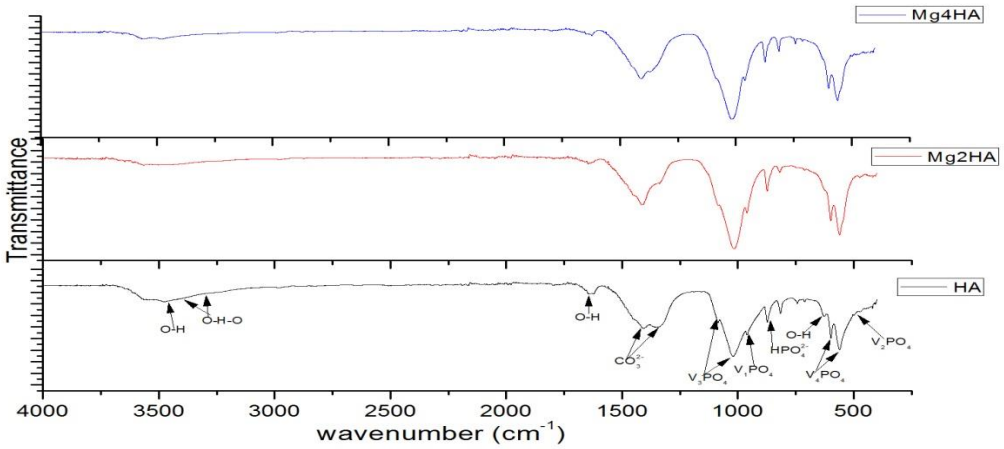

Fig 2:- FT-IR of HA, Mg2HA and Mg4HA

The XRD patterns of HA, Mg2HA and Mg4HA have been shown in Fig. 3. All the crystalline phases observed from the XRD patterns were matched with the (JCPDS) cards. The percentages belonging to HAP and β-TCP phases are listed in

Table 2. Using the XRD data, the crystallite size (X_s), crystallinity percent (X_C %), Ca/P ratio and lattice parameters ('a' & 'c') has been calculated and given in Table 2.

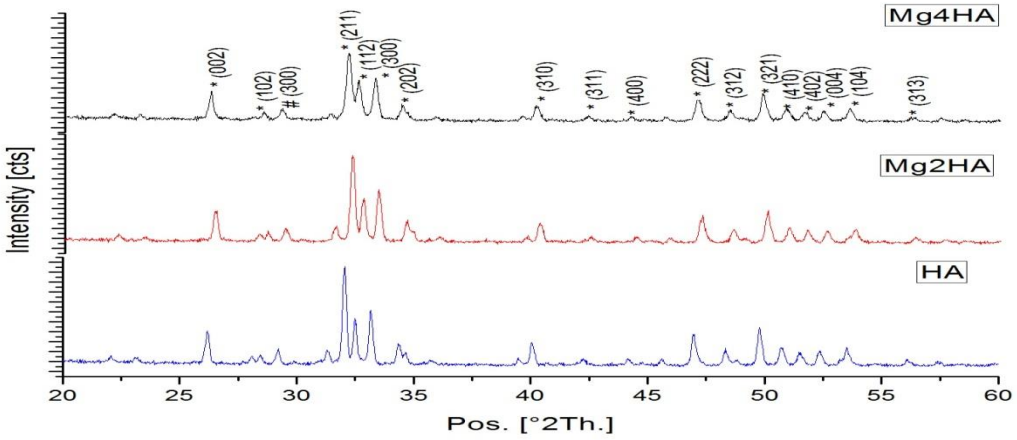

Fig 3: XRD Overlapping of HA, Mg2HA and Mg4HA

Table 2: The parameters calculated from XRD patterns

Sample	HAP (%)	B-TCP (%)	c	a	c/a	(Ca+Mg)/P ratio	Crystallite size (X_s)	Crystallinity (X_c %)
HAP	79	21	6.882	9.4000	0.7319	1.61	38.30	94.20
Mg2HA (0.02M)	74	25	6.862	9.3826	0.7313	1.62	24.77	83.06
Mg4HA (0.04M)	64	36	6.861	9.3810	0.7303	1.60	22.67	75.40

As the ionic radius of magnesium is lower than the ionic radius of calcium due to which it distorts the structure and it results in decrease in lattice parameters [7]. It can also be seen from table that crystallite size of magnesium doped hydroxyapatite is smaller as compared to the undoped hydroxyapatite [9]. The crystallinity percent (X_C%) for the samples has been determined by the following relation [9] and the values are shown in the Table 2.

$$X_C\% = \left(1 - \frac{V_{112/300}}{I_{300}}\right) \times 100$$

The XRF pattern of Mg2HA and Mg4HA is shown in Fig. 4 and the elemental composition is given in Table 3. The doping of magnesium in hydroxyapatite nanopowder is thus confirmed from XRF results. The amount of magnesium in hydroxyapatite was 1.28% and 1.63% for Mg2HA and Mg4HA, respectively, which is same as the amount added during synthesis. Moreover, the results indicate the (Ca+Mg)/P ratio of powder was 1.89 and 1.94 for Mg2HA and Mg4HA, respectively, which indicates that HA formation is incomplete

Table 3: Concentrations of elements in Mg-HA

Samples	**Ca**	**P**	**O**	**Mg**
Wt% in Mg2HA	40.03	16.80	36.60	1.28
Wt% in Mg4HA	34.34	15.8	38.60	1.63

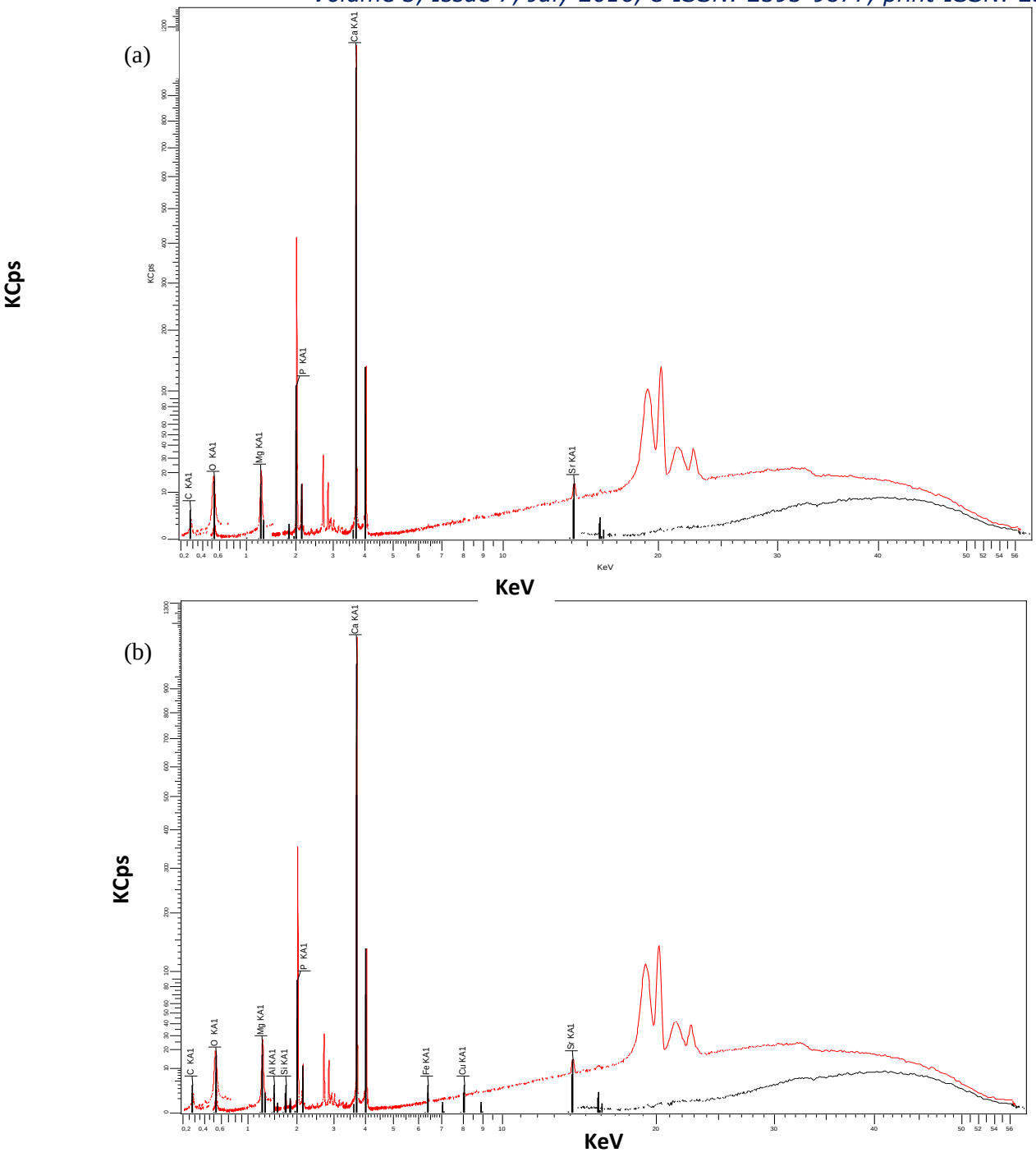

Fig 4: XRF results of (a) Mg2HA and (b) Mg4HA

3.2 Morphological study of coated samples

Morphological studies of HA, Mg2HA and Mg4HA coated samples are shown in Figure 4 which shows Field emission scanning electron microscopy (FE-SEM). FE-SEM images confirmed that HA, Mg2HA and Mg4HA coatings are successfully deposited on substrates. It can be seen from FE-SEM images that coatings are uniform and porous but Mg4HA has relatively dense coating. HA samples composed of irregular rod like shaped particles.

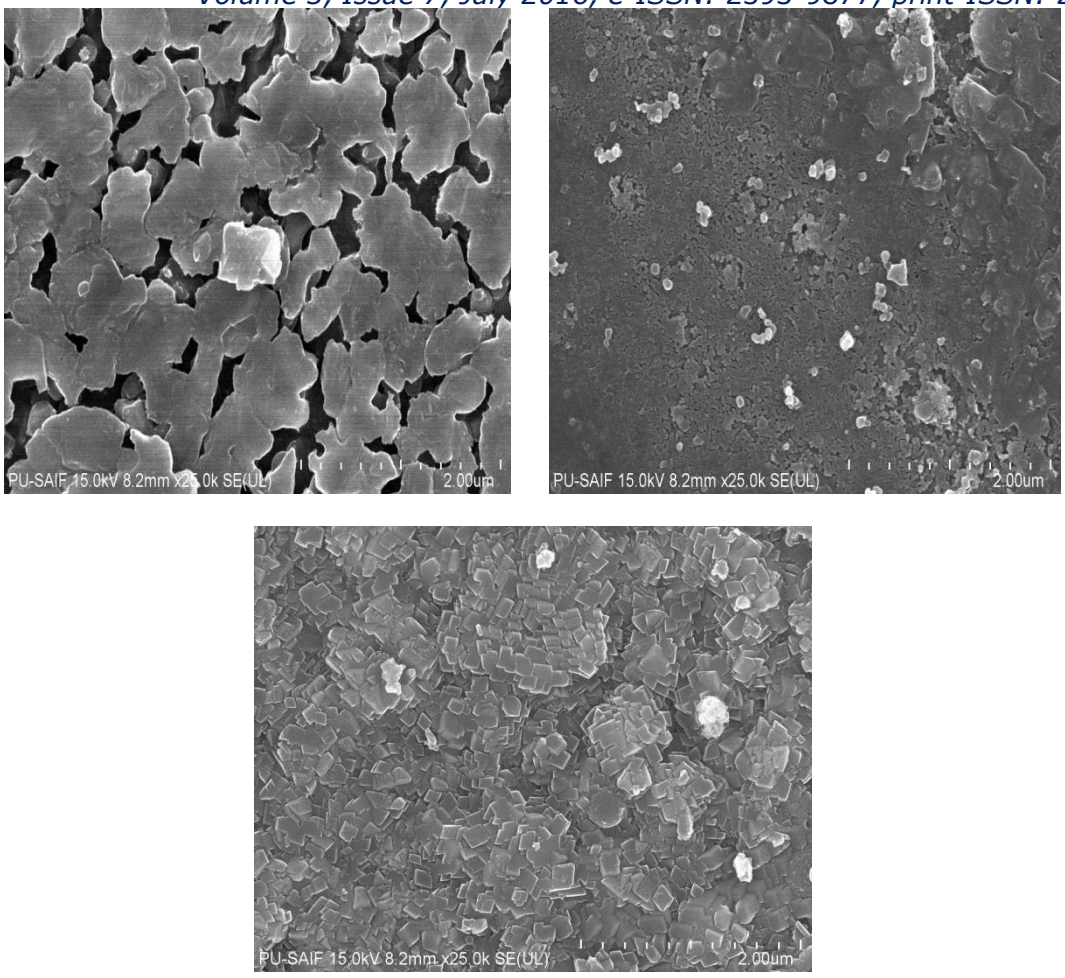

Fig. 4: FE-SEM images of (a) HA (b) Mg2HA (c) Mg4HA

Fig. 5 represents the linear potentiodynamic polarization curves of uncoated 316L SS, HA coating, Mg2HA coating and Mg4HA coating. Higher OCP values of Mg4HA among bare SS, HA and Mg2HA demonstrated that HA coatings were successfully provided a protective layer over 316L SS surface, thus preventing the occurrence of corrosion. Current density of Mg4HA is also low due to which they has low corrosion rate as corrosion rate directly depends on current density.

Table 4: Corrosion parameters from potentiodynamic polarization tests for (a) Bare SS (b) HA (c) Mg2HA (d) Mg4HA

Sample	OCP (V)	b_a (mV/decade)	b_c (mV/decade)	E_{corr} (V)	I_{corr} (μA/cm^2)	Corrosion rate(mm/year)
Bare SS	-0.233	325.72	627.38	-429.86	8.44670	0.098
HA	-0.192	155.32	329.40	-327.84	4.70540	0.056
Mg2HA	-0.179	59.12	109.36	-252.32	3.23560	0.030
Mg4HA	-0.173	86.48	398.67	-226.48	1.54250	0.010

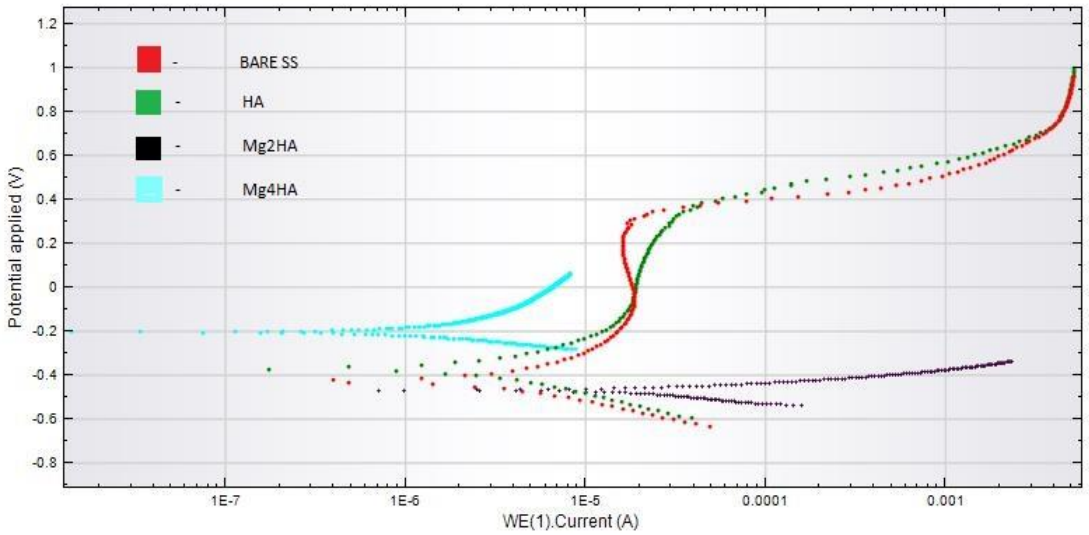

Fig 5: Comparison of Potentiodynamic linear polarization curves of bare SS, HA, Mg2HA and Mg4HA

3.3 Mechanical properties of coated samples

The average surface roughness (Ra), vicker's micro hardness and adhesion strength of bare SS, HA, Mg2HA and Mg4HA are given in Table 5. It can be seen that Mg4HA has high micro hardness and adhesion strength and low surface roughness.

Table 5: Average surface roughness (Ra), vicker's micro hardness and adhesion strength of bare SS, HA, Ag2HA and Ag4HA on 316L SS coatings

Sample	Surface Roughness, R_a (µm)	Vicker's microhardness (VHN)	Adhesion strength
HA	0.141	118.3	39.43
Mg2HA	0.103	121.1	40.36
Mg4HA	0.087	123.6	41.20

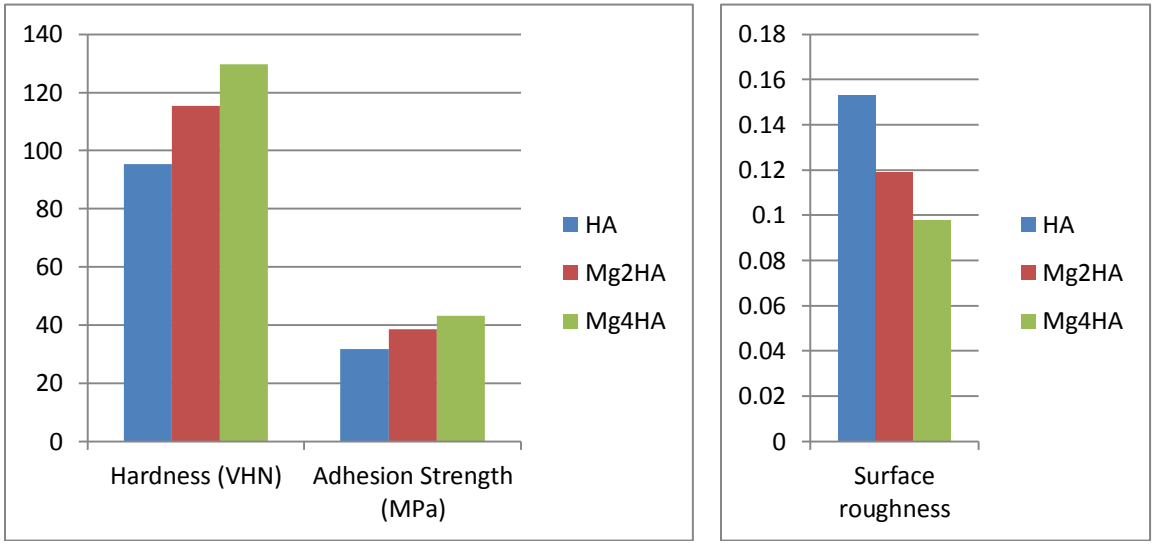

Fig 6: Comparison of surface roughness, Vicker's micro hardness and Adhesion strength of the HA, Mg2HA and Mg4HA

Conclusions

1. Magnesium has been doped successfully in HA and doped amount is equal to the amount added initially during synthesis
2. HA, Mg2HA and Mg4HA coatings have been successfully deposited on 316L SS using sol-gel spin coating technique.
3. All coatings were uniformly spread over the substrate and porous.
4. The corrosion rate of 316L SS, HA coatings, Mg2HA coatings and Mg4HA coatings following a decreasing order; Mg4HA > Mg2HA > HA > 316L SS.
5. The micro hardness of HA coatings, Mg2HA coatings and Mg4HA coatings following a decreasing order; Mg4HA > Mg2HA > HA.
6. The adhesion strength of HA coatings, Mg2HA coatings and Mg4HA coatings following a decreasing order; Mg4HA > Mg2HA > HA.
7. The surface roughness of HA coatings, Mg2HA coatings and Mg4HA coatings following a decreasing order; HA > Mg2HA > Mg4HA.

References:

1. Cheng, K., Gaorong H., Wenjian W., & Haibo Q., Sol-gel derived fluoridated hydroxyapatite films. *Materials Research Bulletin, vol. 38*, pp.89-97, (2003).
2. Disegi, J.A., Eschbach, L., Stainless steel in bone surgery. Injury, *International Journal of the Care of Injured, vol. 47*, issue-7, (2000).
3. Farzadia, Arghavan., Bakhshib, Farhad., Solati-Hashjina, Mehran., Azuan, Noor., Osman, abu., Magnesium incorporated hydroxyapatite: Synthesis and structural properties characterization, *Ceramics International vol. 40*,pp. 6021–6029, (2014).
4. Garcı´a, C., Cere, S., Duran, A., Bioactive coatings prepared by sol–gel on stainless steel 316L, *Journal of Non-Crystalline Solids, vol. 348*, pp. 218–224, (2004).
5. Gerber, I., "Metallic Medical Implants : Electrochemical Characterization of Corrosion Processes," *Metallic implants, vol. 12*, pp. 35–40, (2008).
6. Gozalian, A., Behnamghadera, A., Daliri, M., Moshkforoushc, A., Synthesis and thermal behavior of Mg-doped calcium phosphate nano powders via the sol gel method, *Scientia Iranica vol. 18*, pp. 1614–1622, (2011).
7. Kannan, S., Balamurugan, A., Rajeswari, S., *Electrochimica acta, vol. 50 (10),* pp.2065-2072, (2005).
8. Kanzaki, N., Onuma, K., Treboux, G., Tsutsumi, S., Ito, A., Inhibitory effect of magnesium and zinc on crystallization kinetics of hydroxyapatite, *Biomaterials vol. 22, Issue 21*, pp. 2921–2929, (2001).
9. Kaygili, Omer., Keser, Serhat., Sol–gel synthesis and characterization of Sr/Mg, Mg/Zn and Sr/Zn co-doped hydroxyapatites, *Materials Letters vol. 141*, pp.161–164, (2015).